Journal of Non-Newtonian Fluid Mechanics 231 (2016) 68–78

Contents lists available at ScienceDirect

Journal of Non-Newtonian Fluid Mechanics

journal homepage: www.elsevier.com/locate/jnnfm

Experimental investigation of the impact of elastic turbulence on heat transfer in a serpentine channel

Waleed M. Abed[a], Richard D. Whalley[a,b], David J.C. Dennis[a], Robert J. Poole[a,*]

[a] School of Engineering, University of Liverpool, Brownlow Street, L69 3GH, United Kingdom
[b] School of Mechanical and Systems Engineering, Newcastle University, NE1 7RU, United Kingdom

ARTICLE INFO

Article history:
Received 17 July 2015
Revised 4 March 2016
Accepted 6 March 2016
Available online 12 March 2016

Keywords:
Elastic turbulence
Serpentine channel
Micro-mixing
Convective heat transfer
Viscoelasticity
Shear-thinning effects
Boger fluids

ABSTRACT

The characteristics of convective heat transfer and fluid flow within a square cross-section serpentine channel are experimentally studied for two groups of polymeric viscoelastic fluids, shear-thinning and constant-viscosity Boger solutions. The elastic turbulence can be created by the non-linear interaction between elastic stresses generated within the flowing high-molecular-weight polymer solutions and the streamline curvature. In order to confirm elastic turbulence in this geometry, pressure drop across the serpentine channel was measured. The findings indicate that the measurements of non-dimensional pressure-drop increase approximately from 1.48 to 4.82 for viscoelastic solutions compared with the Newtonian fluid over a range of Weissenberg number from 4 to 211. The convective heat transfer enhances due to elastic turbulence by up to 200% for low polymer concentration (dilute) solutions and reaches up to 380% for higher polymer concentration (semi-dilute) solutions under creeping-flow conditions in comparison to that achieved by the equivalent Newtonian fluid flow at low Graetz number (up to 14.6). We propose a modified Weissenberg number which is able to approximately collapse the mean Nusselt number data for each solution group.

1. Introduction

The practical applications of micro-scale systems, such as bio-engineering devices, microelectronic devices, cooling systems of computer chips and mini or micro-scale heat exchangers have recently received a great deal of attention due to the development of fabrication technologies for these systems. In the micro-scale systems (with "small" dimensions approximately less than 1000 microns), however, flow of Newtonian fluids at very low Reynolds numbers, Re ($\equiv \rho UD/\eta < 1$ where ρ and η are fluid density and dynamic viscosity, respectively, U is a characteristic velocity scale and D is a characteristic length scale) is inherently laminar and steady [1]. As a consequence, mixing at the micro-scale is difficult to achieve (as molecular diffusion is dominant) and thus the enhancement of convective heat transfer is problematic under these conditions. One of the proposed approaches to enhance heat transfer in these conduction-dominated regimes is to use viscoelastic fluids, which are prepared by adding a small amount of high molecular-weight polymer to a Newtonian solvent, in order to introduce non-linear effects and promote the appearance of instabilities even at low Re. Viscoelastic fluid flows in such geometries have then been seen to exhibit "turbulent-like" characteristics such as chaotic and randomly fluctuating fluid motion across a broad range of spatial and temporal scales and have led this to be called "*elastic turbulence*" [2–10].

The concept of elastic instability appeared as a well-known phenomenon for viscoelastic fluid flows in the 1990s. Larson et al. [11] reported theoretical and experimental results that showed that purely-elastic instabilities can arise in viscoelastic fluid flows by a coupling of the first normal-stress difference and streamline curvature. This seminal work was followed by a series of experimental investigations that used different geometries containing curved streamlines to study elastic instabilities in low Re fluid flows. This included swirling flow between parallel disks [2–4], in serpentine or wavy channels [3,5–8] and in concentric cylinder devices [3,9]. Elastic instabilities and resulting non-linear interactions between elastic stresses generated within the flowing high-molecular-weight polymer solutions and the streamline curvature are "purely-elastic" in nature, driven by the elastic (normal) stresses developed in the flow and occur at Reynolds numbers far removed from the usual turbulence observed for Newtonian fluids which is, of course, inertial in nature. Steinberg and co-workers

* Corresponding author Tel.: +44 151 7944806.
E-mail address: robpoole@liv.ac.uk (R.J. Poole).

http://dx.doi.org/10.1016/j.jnnfm.2016.03.003

Table 1
Experimental values of typical Weissenberg number for onset of a purely-elastic instability and elastic turbulence in the serpentine channel flow.

Authors	Weissenberg number range	
	Onset of elastic turbulence	Developed elastic turbulence
Groisman and Steinberg, 2004 [3]	3.2	> 6.7
Burghelea et al., 2004 [6]	1.4–3.5	10
Li et al., 2010 [7]	7.5	15

[2,3,5,6] reported that elastic instabilities of highly-elastic fluids can be exploited to augment fluid mixing in serpentine or curved channels. Typically, viscoelastic fluid flows with negligible inertia ($Re < 1$) that have been stretched along curved streamlines can undergo a series of flow transitions from viscometric laminar flow, to clearly chaotic flow, and eventually to fully developed "elastic turbulence". The experimental study by Poole et al. [12] used elastic turbulence in a swirling flow between two parallel disks to create oil-in-polymer-solution emulsions. Their results showed that for Newtonian oil and continuous phase no emulsification occurred at all. While in the case of the viscoelastic oil solutions, at identical conditions, a good emulsion was observed due to the mixing effects of elastic turbulence.

Prior to this understanding of elastic turbulence, Hartnett and co-workers conducted a set of experimental [13–15] and numerical [16] investigations to study the fundamental characteristics of fully-developed laminar convective heat transfer under different combinations of thermal boundary conditions using various types of viscoelastic fluids in straight ducts. The results indicated that viscoelastic solutions show higher convective heat transfer as compared to Newtonian fluids flow under identical conditions ($Re = 314–1974$, $Pr = 42.9–79$). These increases are attributed to secondary flows, arising from the second normal-stress differences imposed on the surfaces boundaries, which occur in viscoelastic fluids in laminar flow through rectangular or square cross-section ducts. When the concentration of polymer increases this leads to an increase in the strength of the secondary flow and a decrease in the thermal development entrance length. Further numerical studies [17–20] investigated the impact of such secondary flows on the convective heat transfer of the viscoelastic fluids. The results of these numerical studies were consistent with the original experimental results of Hartnett and co- workers [13–16].

The effects of viscoelastic fluids in micro-scale geometries become significant even for dilute solutions because of the small flow time scales and the high shear rates achievable. Availability of these features in the flow simultaneously makes the *Re* small and the Weissenberg number large, *Wi* ($\equiv \lambda U/D$, where λ is the relaxation time of the viscoelastic fluid), which quantifies non-linear elastic effects. From earlier publications [2–9], purely-elastic instabilities have been observed at low *Wi* (order 1) in a range of flows and, at high *Wi* (order 10), elastic turbulence observed as a result of the combination of elastic stresses and streamline curvature. Elastic turbulence can arise in the serpentine channel flow at typical *Wi* numbers as shown in Table 1. The possibility of using elastic turbulence to enhance convective heat transfer in a square serpentine microchannel was quantitatively studied by our research group in a short letter [21] utilising a sucrose-based Boger fluid. These initial experimental findings show that elastic turbulence is able to enhance convective heat transfer in the serpentine channel geometry by up to 300% compared to the equivalent Newtonian fluid flow. Very recently Traore et al. [22] studied the role of elastic turbulence in an axisymmetric swirling (von Karman) flow with a cooled lower stationary wall and compared the temperature fluctuations with those of a low diffusivity tracer. PIV measurements for both isothermal and non-isothermal flows revealed no significant effect of the heat transfer process on the flow topology. The results confirmed our own recent results [21], that elastic turbulence can enhance the heat transfer efficiency above the conductive limit although no Nusselt numbers could be determined in the set-up used by Traore et al. [22]. In the current paper, we give a more complete account of our experiments on the convective heat transfer in the square serpentine microchannel using elastic turbulence as well as studying the influences of both viscoelasticity and shear-thinning viscosity individually on the convective heat transfer by adjusting the solvent viscosity, polymer concentration and imposed shear rate.

2. Experimental setup

The experimental rig that has been used to investigate the behaviour of the flow and convection heat transfer of viscoelastic fluids is shown in Fig. 1. It consists of a copper serpentine channel which is mounted on a plastic frame (PVC) that includes reservoirs at either end of the channel that contains pressure tappings. The fluid is pumped through the serpentine channel using a pressure vessel where the amount of driven liquid flows between an upstream reservoir and a downstream reservoir and then to a collection container where it can be weighed for measuring the flow rate. This pressure vessel is connected to a compressed air supply, which is used to control the flow rate. A Denver Instrument TP-1502, which has an uncertainty ± 0.03 g at stable load, was used to measure the flow rate by weighing the amount of collected fluid with time.

The square cross-section serpentine channel, which was comprised of 20 half-loops with inner and outer radii of $R_i = 1$ mm and $R_o = 2$ mm, respectively, was configured in a (20 mm × 84 mm) piece of copper as shown in Fig. 2. The channel had a square cross-section $W = 1.075 \pm 0.01$ mm (measured with a Nikon EPIPHOT TME inverted microscope 100× magnification setting, 1230 pixels = 1 mm) and was smoothly joined on either side by straight channel sections with a total length of 77 mm: see Fig. 2. The upper channel wall was fabricated from 12 mm-thick PVC. Therefore, the copper side and bottom walls of the serpentine channel were considered to be isothermal whereas the upper wall was adiabatic.

The measurements of pressure drop along the channel are obtained via two pressure taps, which are placed on the upper wall of an upstream reservoir and a downstream reservoir, using a wet-wet Validyne DP15-26 differential pressure transducer. The pressure transducer utilised two different diaphragms to cover the full working range of $0 < \Delta P < 200$ kPa. The voltage output of each of the diaphragms was periodically calibrated for the differential pressure range of $0 < \Delta P < 20$ kPa and the other range of $0 < \Delta P < 200$ kPa using an MKS Baratron differential pressure transducer and both are accurate to $\pm 0.25\%$ full scale. The pressure-drop reading was electronically sampled by an analogue to digital converter at 100 Hz for 60 s after reaching steady-state conditions (approximately 30 min per flow rate). Measurement of the pressure in the reservoirs meant that issues related to hole-pressure error were minimised but resulted in any fluctuation information being severely damped: thus our pressure-drop data is restricted to mean values.

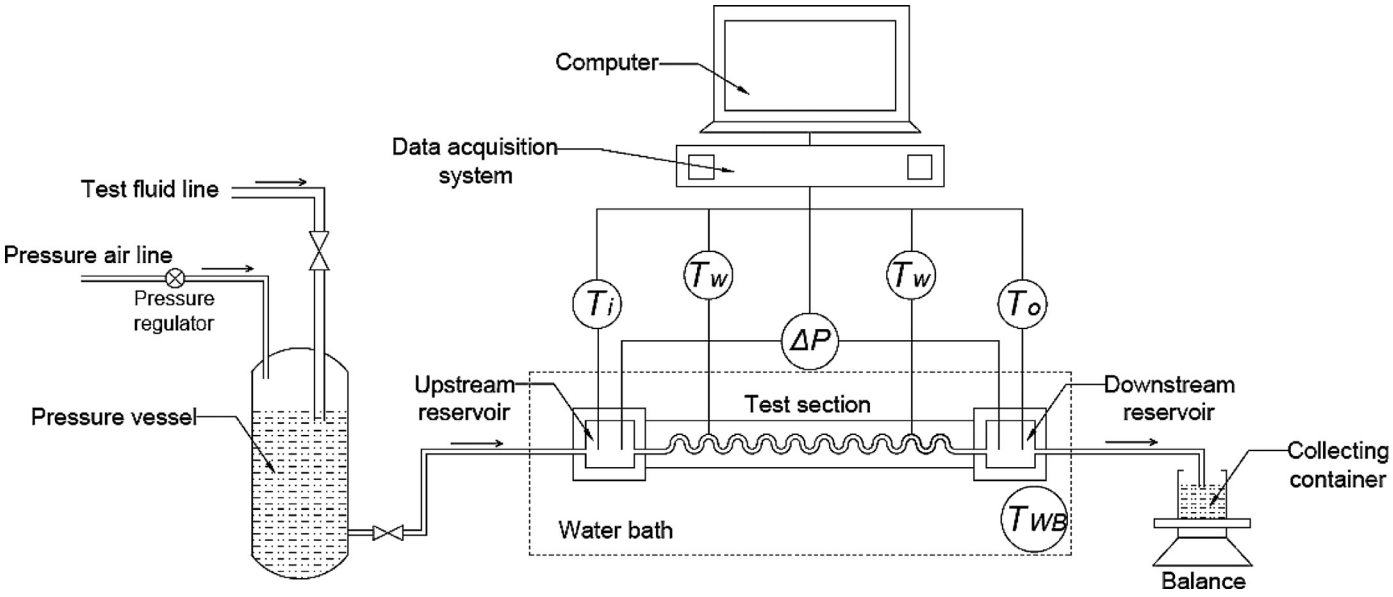

Fig. 1. Schematic diagram of the experimental set up.

K-type thermocouples were positioned in the upstream reservoir and the downstream reservoir for measuring the temperature of the fluid flowing before and after the serpentine channel. Further, four K-type thermocouples were embedded at axial locations along the side walls in both sides at a distance of 1 mm from the wall of the serpentine channel to monitor the wall temperature of the serpentine channel as shown in Fig. 2(b). The side walls and the bottom of the channel were made of copper ($k_{Cu} = 385$ W/m K), therefore they are maintained at essentially isothermal boundary conditions whereas the insulating properties of the PVC ($k_{PVC} = 0.25$ W/m K) ensured an adiabatic boundary condition on the upper wall. The large thermal conductivity of the copper ensured that, although the "wall" temperature was actually measured 1 mm away, the error associated with this assumption was very small. Additional temperature measurements at 8 mm from the wall suggested that the "true" wall temperature (determined by extrapolation) agreed with the assumed value to within 0.01 °C (see Table 2 for more details). The readings of all these thermocouples were electronically recorded over a period of 60 s at a frequency of 100 Hz once steady-state conditions had been obtained. Measuring the temperature in the reservoirs removed any issues regarding physically disturbing the flow in the serpentine channel but, like the pressure-drop data, restricted the data collection to mean values. The thermocouples, which had an accuracy of approximately ± 1°C, were calibrated against a mercury thermometer of certified accuracy (± 0.1 °C) in the range 0 °C–80°C. The whole facility was placed in a Techne TE-10A water bath continuously-stirred and maintained at a temperature of 30°C to achieve constant temperature boundary conditions to the copper walls (in reality the measured wall temperature remained constant to 30 ± 0.2 °C). Typical inlet temperatures were 22 ± 0.5 °C whilst the outlet temperature varied depending on conditions between 24 and 30 °C.

Executing a standard error analysis, the averaged values of uncertainties for friction factor-Reynolds number product, *fRe*, and Nusselt number, *Nu*, were conducted by following the same approach as adopted in Ref. [23]. The minimum and maximum uncertainty values of *fRe* and *Nu* are provided in Table 3 for all working fluids. The greatest uncertainty in determining *Nu* came from the measured temperatures of the walls and fluid at the inlet and outlet serpentine channel (approximately 90% of the total error of the averaged *Nu*), whilst the flow rate and the serpentine channel dimensions contribute about 10% to the total error of the averaged *Nu*. As will be shown, the agreement between the averaged *Nu* from the present experiments for Newtonian fluids and numerical data [23,24] (see Fig. 12) will suggest that these are conservative estimates for the experimental uncertainty and, in reality, the uncertainty in the thermocouple values (and ultimately the averaged *Nu*) is lower than these values in Table 3 suggest.

Finally we confirmed that any contributions from natural convection in our set-up are expected to be negligible, with estimates of typical Grashof numbers (i.e. the ratio of buoyancy to viscous forces) being 10^{-3}. Thus, buoyancy forces are essentially negligible for all of the results shown here.

3. Working fluids preparation and rheological characteristics

A high-molecular-weight polyacrylamide (PAA) ($M_w \sim 1.8 \times 10^7$ g/mole, Polysciences) was dissolved at different concentrations in two types of Newtonian solvents to produce two groups of viscoelastic fluids [25]. The first type of Newtonian solvent, which was a mixture of 10% distilled water and 90% glycerine (1.26 relative density, ReAgent Chemical Services) by weight (hereafter W/GLY mixture), was used to prepare shear-thinning solutions. The second Newtonian solvent, which was an aqueous solution of 65% sucrose (Biochemical grade, 190–192 °C melting point, Sucrose ACROS Organics) and 1% sodium chloride (NaCl) in distilled water all by weight (hereafter W/SUC solution), was employed to prepare approximately constant-viscosity elastic solutions, usually called Boger fluids [26]. Therefore, the effects of shear-thinning viscosity are investigated by dissolving small amounts of PAA in a W/GLY solvent whilst approximately constant-viscosity elastic liquids are studied by adding small amounts of PAA to a W/SUC solvent.

Three shear-thinning solutions containing 50 ppm, 100 ppm and 200 ppm concentration by weight of the PAA dissolved in the aqueous glycerine mixture were prepared. These shear-thinning solutions are henceforth referred to as 50-W/GLY, 100-W/GLY and 200-W/GLY, respectively. The Boger solutions were produced by dissolving 80 ppm, 120 ppm and 500 ppm concentration by weight of the same polymer in the aqueous sucrose solution, are hereafter referred to as 80-W/SUC, 120-W/SUC and 500-W/SUC respectively.

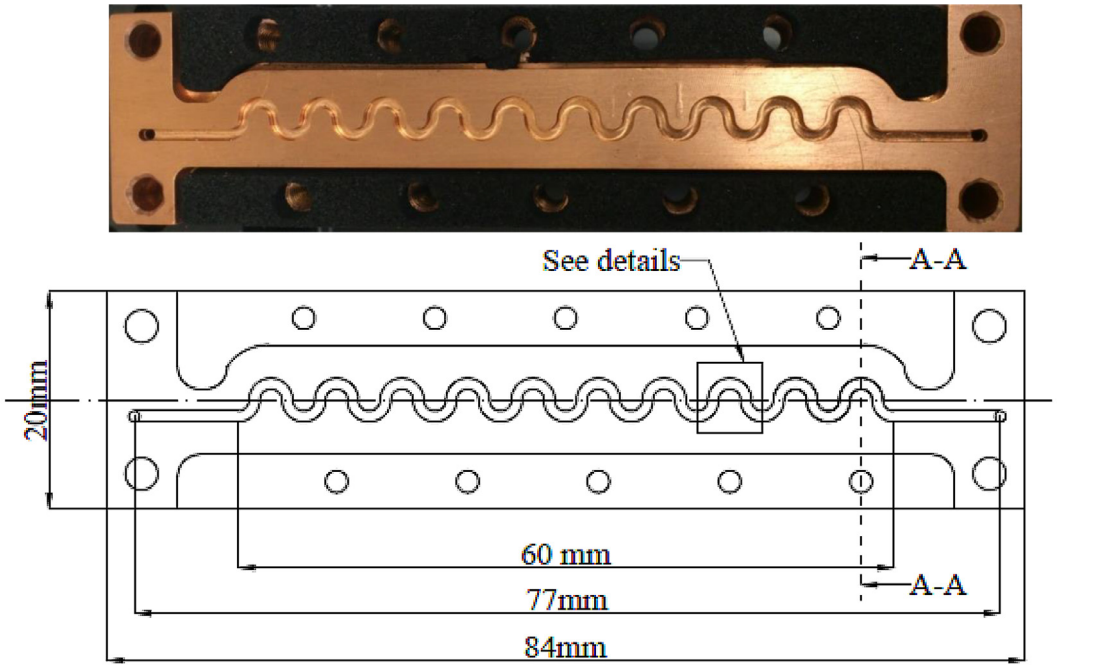

(a) Plan view

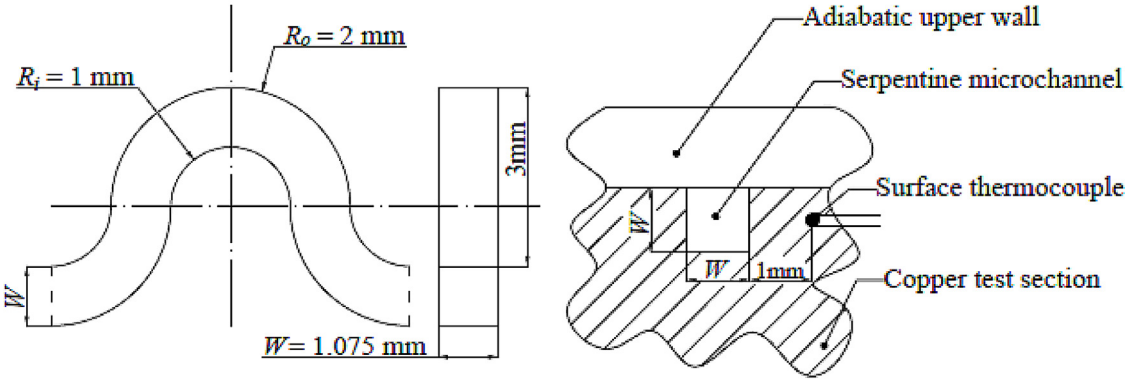

(b) Details and cross-sectional view

Fig. 2. Schematic diagram of the serpentine channel.

Table 2
The measurements of the wall temperature of the serpentine channel at two different positions within the wall.

Water bath temperature (°C)	Average temperature at 1 mm from wall (°C)	Average temperature at 8 mm from wall (°C)	Extrapolated internal surface temperature (°C)
17.5	17.41	17.43	17.407
29.5	29.34	29.42	29.330
39.2	38.95	39.05	38.937

Table 3
Minimum and maximum uncertainty values of *fRe* and $\overline{Nu}$.

Working solutions	*fRe* uncertainty		$\overline{Nu}$ uncertainty	
	Min. (%)	Max. (%)	Min. (%)	Max. (%)
W/GLY	2.73	6.51	8.01	9.78
50-W/GLY	2.88	7.21	8.37	10.84
100-W/GLY	3.42	10.42	11.65	13.14
200-W/GLY	4.04	16.70	12.98	16.78
W/SUC	2.77	4.26	8.17	9.97
80-W/SUC	2.96	5.67	8.96	11.05
120-W/SUC	3.25	14.70	12.23	13.79
500-W/SUC	4.55	16.37	15.01	19.29

Table 4 provides an overview of the composition of the studied solutions.

All rheological measurements for Newtonian (solvents) and viscoelastic solutions were conducted using a TA Instruments AR1000N controlled-stress rheometer with an acrylic cone-and-plate geometry (60 mm diameter, 2° cone angle) with an uncertainty in viscosity of ± 2% [27].

The shear viscosity, η, for all viscoelastic solutions against shear rate, $\dot{\gamma}$, is illustrated in Fig. 3 at 20 °C. The Carreau–Yasuda model [28] was adopted to fit the experimental viscosity data:

$$\eta_{CY} = \eta_\infty + \frac{(\eta_o - \eta_\infty)}{\left[1 + (\dot{\gamma}_{CY})^a\right]^{n/a}} \quad (1)$$

Table 4
An overview of the working fluids.

Working solutions	PAA concentration	Solvent (X+H_2O)		NaCl
	ppm	X	%	%
W/GLY	–	Glycerine	90	–
50-W/GLY	50	Glycerine	90	–
100-W/GLY	100	Glycerine	90	–
200-W/GLY	200	Glycerine	90	–
W/SUC	–	Sucrose	65	1
80-W/SUC	80	Sucrose	65	1
120-W/SUC	120	Sucrose	65	1
500-W/SUC	500	Sucrose	65	1

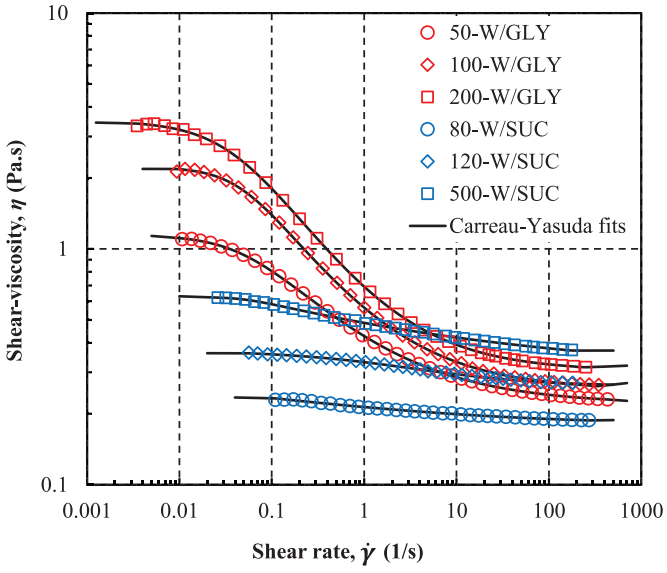

Fig. 3. Shear-viscosity versus shear rate for PAA-W/GLY and PAA-W/SUC solutions. Black lines are Carreau–Yasuda fits [28] with parameters shown in Table 5.

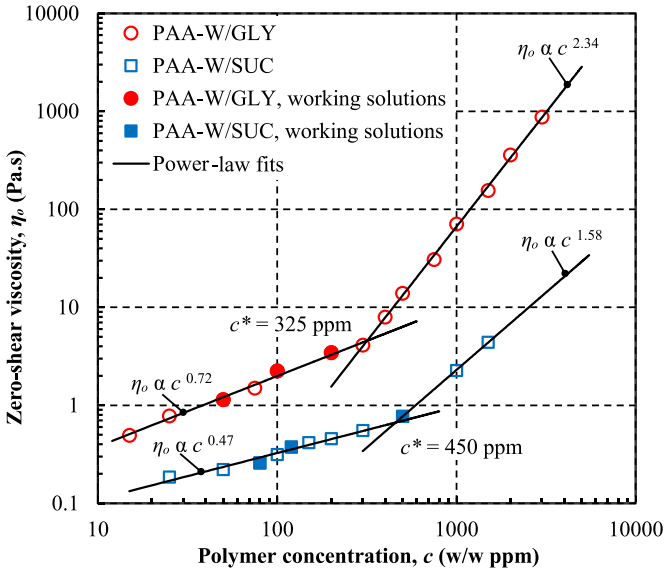

Fig. 4. Extrapolated zero-shear viscosity versus polymer concentration for PAA-W/GLY and PAA-W/SUC solutions.

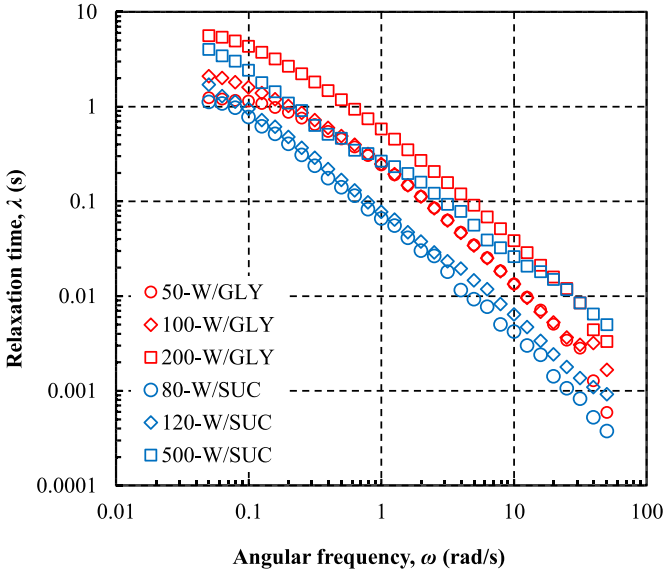

Fig. 5. Relaxation time obtained from small amplitude oscillatory shear stress measurements for PAA-W/GLY and PAA-W/SUC solutions.

where, η_o, η_∞ are zero-shear-rate viscosity and infinite-shear-rate viscosity, respectively, λ_{CY} is a constant that represents the inverse shear rate at the onset of shear-thinning, a is a fitting parameter introduced by Yasuda et al. [28] and n is a power law index. All fitting parameters for the Carreau–Yasuda model, which are tabulated in Table 5, have been determined using the least-squares-fitting method outlined in Escudier et al. [27]. Fig. 3 shows that both viscoelastic solutions exhibit shear-rate dependent viscosity. However, the PAA-W/GLY solutions possess significantly greater shear-thinning effects than the PAA-W/SUC solutions.

The critical overlap concentration, c^*, which corresponds to the approximate concentration when the polymer coils in solution begin to overlap with each other [29,30], has been determined by plotting in log–log form the zero-shear viscosity, η_o, versus a wide range of PAA concentrations as shown in Fig. 4. Therefore, the viscoelastic solutions can be characterised as dilute solutions ($c < c^*$) or semi-dilute solutions ($c > c^*$) depending on the value of c^*. As can be seen from Fig. 4, the critical overlap concentration for the shear-thinning solutions over a range of fourteen concentrations from 15 ppm to 3000 ppm (w/w) is approximately 325 ppm whilst for the Boger solutions over a range of eleven concentrations from 25 ppm to 1500 ppm (w/w), it is around 450 ppm at 20 °C. Concentrations of working fluids for both shear-thinning solutions and Boger solutions can be regarded as dilute solutions with the exception of 500-W/SUC, which can be considered as a semi-dilute solution ($c/c^* \sim 1.1$). The non-dimensional concentration, c/c^*, for all working fluids are provided in Table 5.

Small amplitude oscillatory shear stress (SAOS) tests were used to measure the storage modulus, G', which measures the energy of elastic storage and the state of the structured materials, and the loss modulus, G'', which represents viscous dissipation or loss of energy. Therefore, for Newtonian fluids (or any inelastic fluids) the relaxation time, λ, is equal to zero and this leads to $G' = 0$ and $G'' = \mu\omega$, where ω is the angular velocity (rad/s). A frequency sweep is carried out within the linear viscoelastic region (such that the oscillation frequency is changed while the oscillatory shear stress is kept constant at a low value such that the results are independent of the precise stress value applied). Fig. 5 shows the frequency/shear-rate dependent polymer relaxation time ($\lambda = G'/G''\omega$) from the measurements of SAOS for all working solutions at 20 °C. The values of the longest relaxation time, λ_o, which are estimated in the limit of the angular velocity approaching to zero, are also summarised in Table 5 for all working fluids. Moreover, an additional procedure has also been carried out to estimate

Table 5
Rheological properties for all working fluids. (All data at 20 °C).

Working solutions	η_o (Pa s)	η_∞ (Pa s)	λ_{CY} (s)	a (Dimensionless)	n (Dimensionless)	c/c^* (Dimensionless)	λ_o (s)	$\bar{\lambda}_{Maxwell}$ (s)	λ_{Zimm} (s)
W/GLY	0.208	–	–	–	–	–	–	–	–
50-W/GLY	1.145	0.220	19.517	1.372	0.501	0.154	1.25	1.22	2.5
100-W/GLY	2.221	0.253	22.122	1.763	0.595	0.307	2.11	2.24	2.5
200-W/GLY	3.487	0.304	25.399	1.205	0.647	0.615	5.64	5.49	2.5
W/SUC	0.160	–	–	–	–	–	–	–	–
80-W/SUC	0.253	0.186	0.564	0.364	0.421	0.178	1.12	0.87	1.4
120-W/SUC	0.369	0.261	0.490	0.434	0.645	0.267	1.71	1.63	1.4
500-W/SUC	0.769	0.348	1.238	0.274	0.490	1.111	4.03	3.87	1.4

the mode-averaged longest relaxation time by applying the experimental data of the storage and loss modulus within a multimode Maxwell model fit [25,31] i.e. $\bar{\lambda}_{Maxwell} = \sum_i^n \lambda_i \eta_i / \sum_i^n \eta_i$ where λ_i are the relaxation modes and η_i the viscous modes (typically three modes were required for a satisfactory fit).

The estimated values of the longest relaxation time for the selected viscoelastic solutions are listed in Table 5 and it can be seen that they are very similar to λ_o. The relaxation time of a dilute polymeric solution can also be evaluated according to Zimm's theory as [32]:

$$\lambda_{\text{Zimm}} = F\frac{[\eta]M_w\eta_s}{N_A k_B T} \tag{2}$$

where N_A is the Avogadro's constant, k_B is the Boltzmann's constant, T is the absolute temperature, M_w is the molecular weight of polymer, η_s is the solvent viscosity and $[\eta]$ the intrinsic viscosity which can be estimated as $[\eta] \sim 1/c^*$ [33] to be 3077 and 2222 ml/g for PAA-W/GLY and PAA-W/SUC, respectively, using the experimentally-determined values of critical overlap concentration. The prefactor F is defined by the Riemann Zeta relationship [33,34] to be $F = \frac{1}{\sum_{i=1}^{\infty}(\frac{1}{i^{3\upsilon}})} \approx 0.5313$, where υ is the solvent quality parameter which can be obtained for a good solvent from the exponent in the Mark-Houwink correlation $[\eta] = KM_w^{(3\upsilon-1)}$ to yield $(3\upsilon - 1) = 0.8 \Rightarrow \upsilon = 0.6$ where, K is equal to 4.9×10^{-3} with intrinsic viscosity in units of (ml/g) and $(3\upsilon-1)$ is equal to 0.8 in water [35]. Therefore, the estimated relaxation times for PAA-W/GLY and PAA-W/SUC are 2.5 s and 1.4 s, respectively. The theoretical Zimm relaxation times obtained can be compared to those determined from the SAOS measured in the cone-and-plate rotational rheometer (see Table 5), showing good agreement.

Fig. 6 shows experimental results of the first normal-stress difference, N_1 ($\equiv \tau_{xx} - \tau_{yy}$) for polymeric solutions at the concentrations used for the convective heat transfer experiments. The data of the first normal-stress difference was fitted with a power-law (the solid lines in Fig. 6) between shear rates $\dot{\gamma} > 10$ (1/s) because of the limited experimental resolution (below the sensitivity of the rheometer) and the shear rates $\dot{\gamma} < 200$ (1/s), above which the shear flow became unstable owing to viscoelastic instabilities. Data were obtained with 20 s of equilibration time at each value of shear rate and over several trials (at least four runs for each sample). The temperature was kept constant at 20 °C by using a Peltier plate to set the temperature of the solution sample to within ± 0.1 °C. The first normal-stress difference can be estimated from the total normal force for a cone-and-plate geometry using [36],

$$N_1 = \frac{2F}{\pi R^2} \tag{3}$$

where F is the total normal force (N) and R is the cone radius (m). The experimental values of normal force for all viscoelastic solutions may be slightly lower than the true values because of inertia effects, which is known as the '*negative normal stress effect*' [31] and was corrected by adding the inertial contributions using

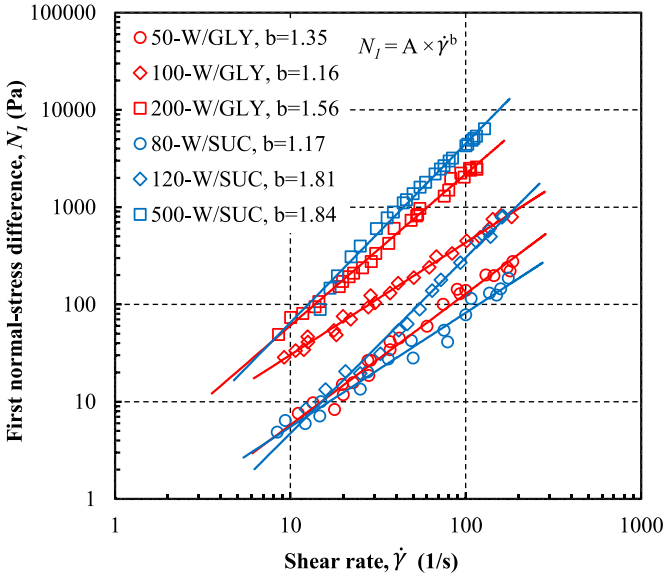

Fig. 6. First normal-stress difference against shear rate for PAA-W/GLY and PAA-W/SUC solutions. Solid lines represent a power-law fit to the normal-stress data.

[36],

$$\Delta F = \frac{3\pi\rho\omega^2 R^4}{40} \tag{4}$$

where ΔF is the difference in the normal force owing to inertia (N), ρ is the density of the sample and ω is the angular velocity (rad/s). A density meter (Anton Paar DMA 35 N) with a quoted precision of 0.001 g/cm^3 was utilised for evaluating the density of the working fluids.

Differential scanning calorimetry (DSC) – Model V24.11 DSC Q2000, TA Instruments, USA – was used to measure the specific heat capacity by the modulated method to obtain a measurement of heat capacity for all selected viscoelastic solutions. The DSC was fully computer-controlled with rapid energy compensation and equipped with automatic data analysis software to calculate heat capacity from the heat flow data. Accuracy and reproducibility of heat capacity measurements on the DSC were first validated with the standard samples of sapphire, which are run under the same conditions that are subsequently used for all samples. The inset of Fig. 7 shows the experimental results of a sapphire sample (sample mass = 22.6 mg and heating rate 2 °C/min.) in the range from 742.1 to 874.2 J/kg °C together with standard sapphire data [37] for temperatures from 10 to 83.3 °C. Comparison with standard sapphire data illustrates that the accuracy of the experimental sapphire measurements was within 0.5%. Fig. 7 displays the experimental specific heat capacity results for both PAA-W/GLY and PAA-W/SUC solutions in the range of temperatures between 10 and 83.3 °C. The data representation has been plotted as an average from at least three runs for each sample. The experimental

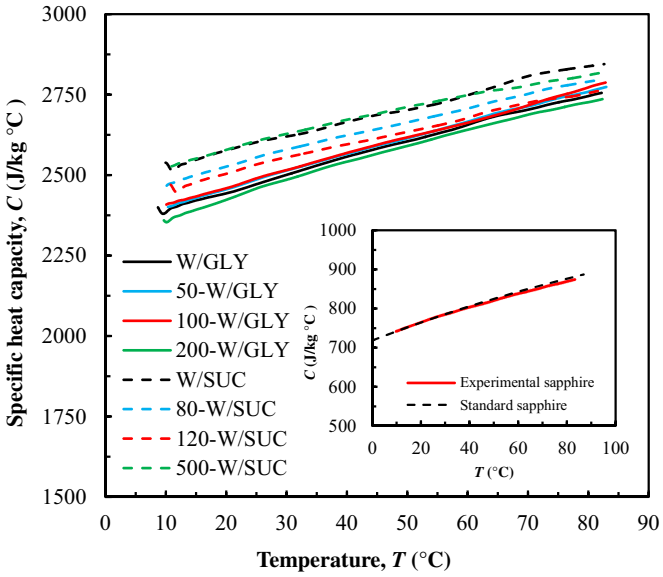

Fig. 7. Typical variation of specific heat capacity for PAA-W/GLY and PAA-W/SUC solutions against temperature. The inset shows the experimental data of a standard sapphire sample with standard sapphire data [37].

results indicate that the specific heat capacities increase gradually with increasing temperature for all viscoelastic solutions. However, the specific heat capacities of PAA-W/SUC solutions are slightly greater than the values of PAA-W/GLY solutions over the entire temperature range. The data in Fig. 7 shows that there is a slight effect from the different polymer concentrations in the chosen viscoelastic solutions on the values of specific heat capacity but no clear trends are apparent and the differences are within the repeatability of the technique for identical fluids. Thus we conclude, for the fluids used here, the addition of polymers to a Newtonian solvent does not alter its specific heat capacity in agreement with previous studies in the literature [38].

The thermal conductivity of the samples W/GLY, 200-W/GLY, W/SUC and 500-W/SUC has been measured using the Fox-50 device, which is a commercial instrument manufactured by Laser-Comp Thermal Conductivity Instrument. Measurements of the thermal conductivity are taken from the thermal contact resistance via the guarded heat flow meter technique. Pyrex was selected to calibrate the Fox-50 device because it is close to the expected value of the thermal conductivities. The experiments were conducted with a temperature difference between the hot and cold plates at 10 °C at two different mean temperatures (10 °C and 40 °C). The average values of the thermal conductivity (at least three runs for each sample) for the selected samples were then determined. The results suggest that the addition of small amounts of polymers has a negligible effect on the values of the thermal conductivities as any small variation in the results is within the uncertainty and repeatability of the measurement (±10%). Therefore, the current results are consistent with the results of Lee et al. [39], who demonstrated that the addition of polymer up to 10,000 ppm (w/w) to Newtonian solvents does not change values of thermal conductivity for these resulting solutions. Therefore, it is possible to use the thermal conductivity values of aqueous glycerine solutions [40] for all PAA-W/GLY solutions and sucrose solution values [41,42] for PAA-W/SUC solutions (see data in Table 6). We note here, that although the negligible effect of dilute polymers on the specific heat capacity and thermal conductivity is in good agreement with the prevalent view in the literature [38], these results are in marked constant to the recent results of Traore et al. [22] where significant differences in the thermal diffusivity are reported for similar solutions to one of those used here (W/SUC).

Finally to estimate the activation energy for each of the two solvents we measured the viscosity across the temperature range used in the experiments (20–30 °C, 293–303 K) and fitted an exponential Arrhenius-type fit to the data. Doing so gives an estimation of the activation energy of 1710 kJ/kg for the glycerol solvent and 1300 kJ/kg for the sucrose solvent indicating a stronger temperature-dependence for the glycerol-based fluids.

4. Results and discussion

The experimental measurements of steady-state pressure drop, ΔP, for all working fluids acquired along the serpentine channel between an upstream reservoir and a downstream reservoir for a range of flow rates between 0.2 ml/min and 24.8 ml/min are presented in Fig. 8. The pressure-drops for the Newtonian fluids exhibit a linear increase across the whole range of flow rates. Fig. 9 shows the Darcy friction factor, $f(\equiv 2\Delta PW/(\rho LU_B^2)$, where U_B is a bulk flow velocity, W and L are the depth and path-length of the square serpentine channel, respectively) versus Re ($\equiv \rho U_B W/\eta_{CH}$, where η_{CH} is the characteristic shear-viscosity, which was obtained at a characteristic shear rate, $\dot{\gamma}_{CH}$ ($\equiv U_B/W$) from the Carreau–Yasuda model fit [28] to the steady-shear viscosity measurements at the mean film temperature equal to $(T_{m,i}+T_{m,o})/2$, where $T_{m,i}$ and $T_{m,o}$ denote the mean (bulk) fluid temperature at the inlet and outlet reservoirs, respectively) for all working fluids. The experimental measurements of friction factor were measured when the upper wall of the serpentine channel was insulated and the side walls were maintained at constant temperature. Fig. 9 indicates that the values of friction factor for Newtonian fluids (W/GLY and W/SUC) collapse with the theoretical (Darcy) equation ($f = 57/Re$, for straight square cross-section ducts [43]) for fully-developed isothermal laminar flow ($Re = 0.2$–5.7) where the friction factor values decline linearly with Re on a log–log plot. Although secondary flow may be generated due to the combination of large axial normal stresses with streamline curvature (e.g., as in the classical paper of Dean [44]), we find here that the Newtonian fluid flow behaves essentially as flow in a straight

Table 6
Thermal properties for all working fluids.

Working solutions	ρ (kg/m^3)	C (J/kg K)		K(W/mK)		Pr(Dimensionless)
		Measured	Ref.	Measured	Ref.	
W/GLY	1233	2477	–	0.305	0.3015 [40]	1296
50-W/GLY	1234	2492	–	–	–	1379
100-W/GLY	1236	2496	–	–	–	1829
200-W/GLY	1237	2454	–	0.285	–	2601
W/SUC	1311	2606	2655 [42]	0.368	0.402 [41]	772
80-W/SUC	1315	2561	–	–	–	1086
120-W/SUC	1315	2538	–	–	–	1253
500-W/SUC	1318	2611	–	0.365	–	1979

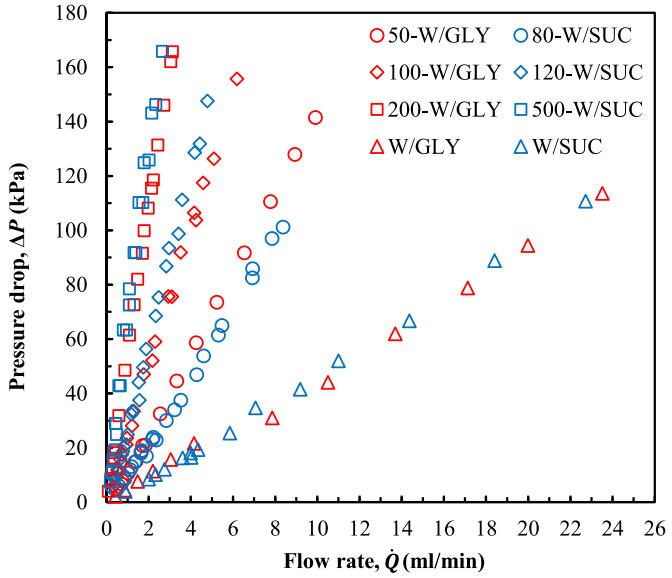

Fig. 8. Pressure-drop measurements versus flow rate for PAA-W/GLY and PAA-W/SUC solutions.

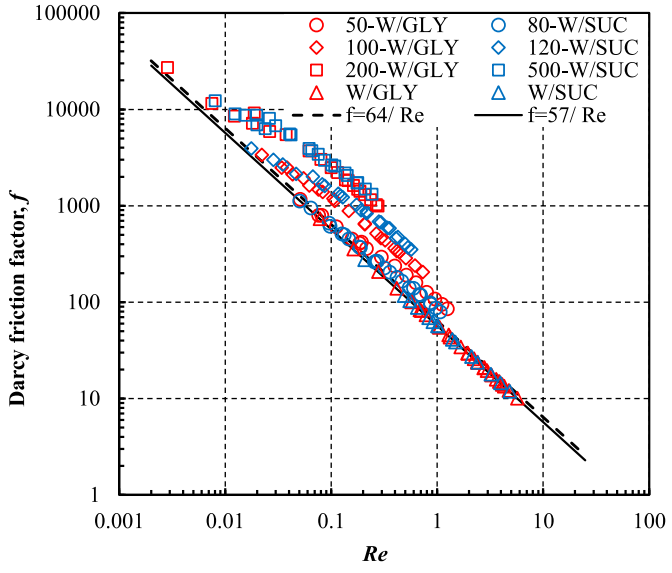

Fig. 9. Darcy friction factor, *f*, versus Reynolds number, *Re*, for PAA-W/GLY and PAA-W/SUC solutions.

channel even within the serpentine channel owing to the dominance of the viscous forces, which suppress the formation of secondary flow [23] (Dean's vortices [44]). The maximum deviation between the measured values of friction factor and the well-known Darcy's formula is within ± 7.6%. Therefore, experiments with Newtonian fluids emphasised the validity of the present experimental techniques and measuring system. In contrast, the friction factor values for viscoelastic solutions, which were selected to understand elastic turbulence effects on heat transfer in the serpentine channel, are also shown in Fig. 9. The measured values of friction factor for these viscoelastic solutions demonstrate a significant increase compared with the Newtonian solution over the same range of *Re*. In the viscoelastic fluid flow (even with very low *Re*) a secondary flow may develop due to the combination of a first normal-stress difference and streamline curvature [45]. However, the large increases in the non-dimensional pressure drop for the viscoelastic solutions are probably attributable to the appearance of "*elastic turbulence*" above a certain flowrate (see e.g. data in Table 1).

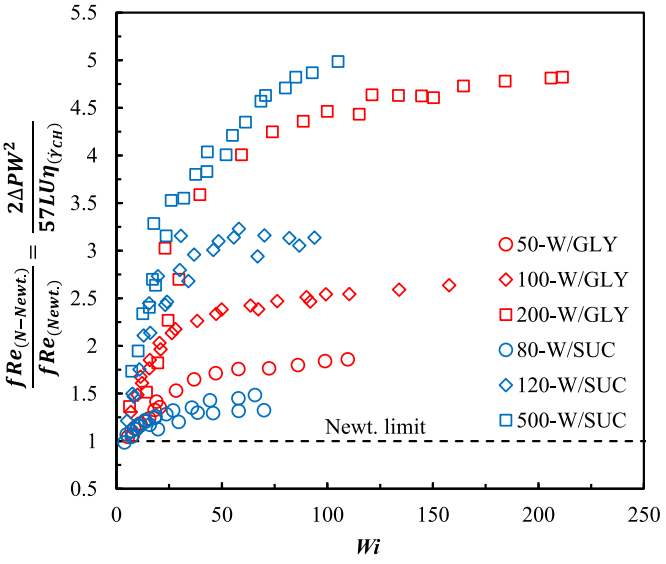

Fig. 10. Normalised friction factor-Reynolds number product, *fRe*, versus Weissenberg number for PAA-W/GLY and PAA-W/SUC solutions.

The friction factor-Reynolds number product – essentially the pressure-drop normalised by a viscous stress – is shown in Fig. 10 as a function of $Wi \equiv \lambda_o \dot{\gamma}_{CH}$, where λ_o is the longest relaxation time, which was evaluated at the mean film temperature. The values of *fRe*, normalised by *fRe* for laminar fully-developed Newtonian fluid flow in a straight square duct ($fRe = 57$), rise rapidly initially with increasing *Wi* before levelling off. From previous publications [3,6–8,45,46], it is known that, creeping flows of viscoelastic solutions ($Re \to 0$) through a serpentine channel develop firstly at low *Wi* to a steady secondary flow [45] before the onset of a purely-elastic instability, which leads eventually to oscillatory time-dependent flow at *Wi* of order one for constant-viscosity fluids ($Wi \sim 3.2$ [3], 1.4–3.5 [6]). Beyond this first purely-elastic instability, the flow becomes increasingly complex and then develops to elastic turbulence, which is observed beyond $Wi > 6.7$ [3], 10 [6], 7.5–15 [7]. Fig. 10 shows that for $Wi < 5$ the pressure drop is similar to that for a Newtonian fluid. With increasing Weissenberg number ($5 < Wi < 25$) the purely-elastic instability develops and leads to an increase in the normalised pressure-drop. The increase in the normalised pressure-drop values for all viscoelastic solutions beyond $Wi \approx 25$ are much greater than the Newtonian limit, suggesting that the complexity of the elastic instabilities increase with increasing *Wi* [21]. The highest non-dimensional values of pressure-drop in terms of normalised *fRe* increase approximately from 1.86 for 50-W/GLY to 4.67 for 200-W/GLY for shear-thinning solutions meanwhile for Boger solutions they range from 1.48 for 80-W/SUC to 4.82 for 500-W/SUC.

Measurements of the temperature difference between outlet and inlet ($T_{m,o}$ - $T_{m,i}$) for viscoelastic solutions (shear-thinning and Boger solutions) versus *Wi* are shown in Fig. 11. The temperature of fluid in the inlet and outlet represent, in fact, the average fluid temperature in the reservoirs of the upstream and downstream of the serpentine channel. As can be seen in Fig. 11, the temperature difference decreases progressively with increasing *Wi* as a consequence of the reduced residence time in the channel. The effect of elastic turbulence on enhancing the heat transfer can most readily be seen for the higher concentration solutions (e.g. 200-W/GLY and 500-W/SUC) where the temperature increase remains approximately constant (approximately 8 °C) despite this reduced residence time.

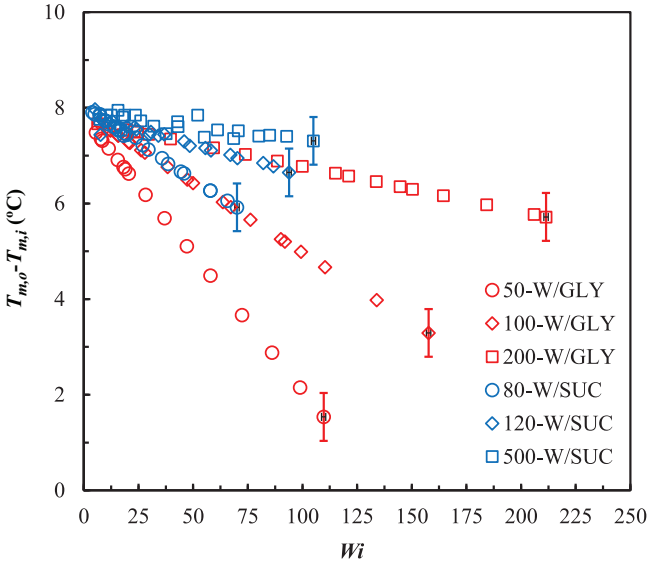

Fig. 11. Temperature difference measurements between outlet and inlet, $T_{m,o}$ - $T_{m,i}$, versus Weissenberg number, *Wi*, for viscoelastic solutions (shear-thinning and Boger solutions).

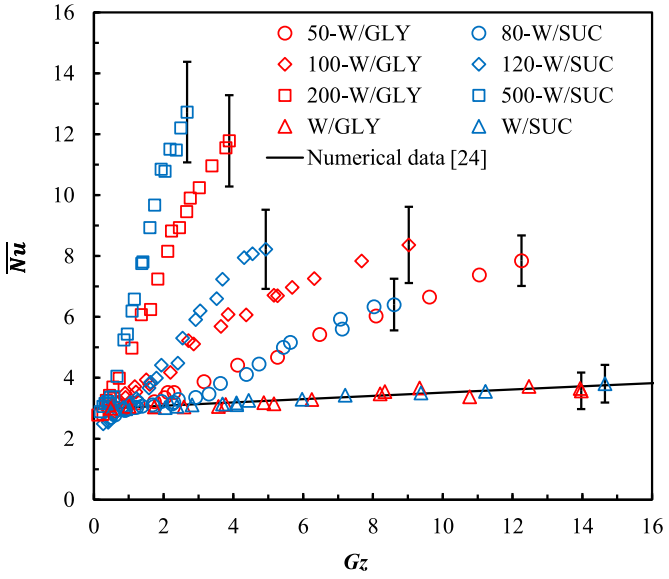

Fig. 12. Mean Nusselt number, $\overline{Nu}$, versus Graetz number, *Gz*, for PAA-W/GLY and PAA-W/SUC solutions.

The enhancement of heat transfer by elastic turbulence can be more fully quantified via the estimation of mean Nusselt number, $\overline{Nu}$, which represents the ratio of convective heat transfer to purely conductive heat transfer between a moving fluid and a solid surface [43], defined as,

$$\overline{Nu} = \frac{\dot{m}CW}{kA_s}\ \frac{(T_{m,o} - T_{m,i})}{\Delta T_{lm}} \tag{5}$$

where $\dot{m}$ denotes the mass flow rate, k and C represent the thermal conductivity and specific heat capacity of the fluid, respectively. A_s is the heated surface area of the square serpentine channel (=458 mm^2). ΔT_{lm} is the *log-mean temperature difference* and is defined as [43]:

$$\Delta T_{lm} = \frac{((T_w - T_{m,o}) - (T_w - T_{m,i}))}{ln\left[\frac{(T_w - T_{m,o})}{(T_w - T_{m,i})}\right]} \tag{6}$$

where T_w is the channel wall temperature.

The mean *Nu* values for Newtonian solutions (W/GLY and W/SUC) and viscoelastic solutions (shear-thinning and Boger solutions) against Graetz number, *Gz* ($\equiv W/L.Re.Pr$, where *Pr* ($\equiv C\eta_{CH}/k$) is Prandtl number where the averaged values of Prandtl number at the mean film temperature for all working solutions are listed in Table 6), are shown in Fig. 12. The averaged *Nu* for Newtonian fluid flow collapses to the numerical predictions [24] for a thermally-developing laminar flow through a straight square duct under the condition of constant wall temperature. The curvature of the serpentine channel has apparently little impact for Newtonian fluid flows at such low *Gz* (up to 14.6). On the other hand, there is a significant increase of the $\overline{Nu}$ for all viscoelastic solutions. It is expected that this enhancement of heat transfer is due to elastic turbulence [3,5–8], which apparently evolves in the flow and results in enhanced mixing [2,5]. Elastic turbulence generated in the flow of viscoelastic solutions is shown to augment the convective heat transfer in the serpentine microchannel by approximately 200% for 50-W/GLY and 80-W/SUC and reaches up to 380% for 200-W/GLY and 500-W/SUC under creeping-flow conditions in comparison to that achieved by the equivalent Newtonian fluid flow at identical Graetz number.

The $\overline{Nu}$ data, normalised by the equivalent $\overline{Nu}$ for a Newtonian fluid in a square duct, is presented against *Wi* in Fig. 13.

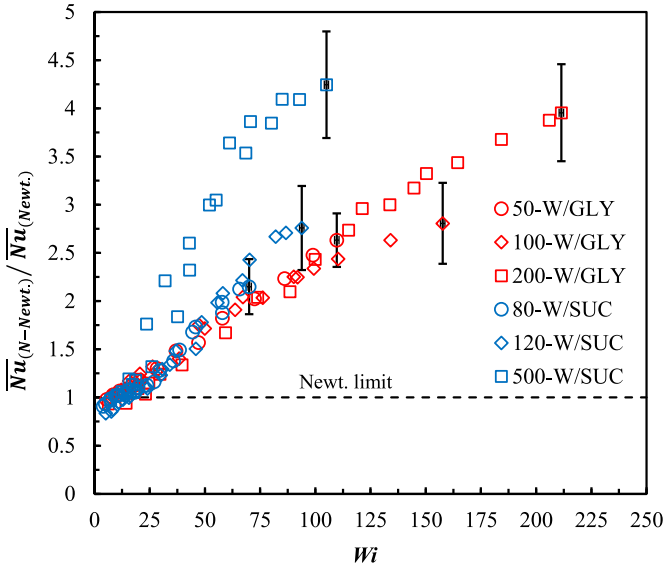

Fig. 13. Normalised Mean Nusselt number, $\overline{Nu}$, versus Weissenberg number, *Wi*, for PAA-W/GLY and PAA-W/SUC solutions.

Fig. 13 shows that the behaviour of viscoelastic flow is essentially Newtonian at very low *Wi* (< 25), and the flow here can be considered to be quasi-viscometric as the secondary flow does not appear to effect *Nu* much. Beyond a critical Weissenberg number, $Wi_c \approx 25$ [3,6,7], the flow undergoes a purely-elastic instability. With increasing *Wi*, the viscoelastic flow evolves to fully-developed "*elastic turbulence*" [3–8]. Thus, we posit that, the increase in convective heat transfer here is due to the influence of such elastic turbulence, which is created by the non-linear interaction between elastic stresses generated within the polymeric solutions and the streamline curvature of the serpentine geometry [3–8]. From Fig. 13, there is an excellent overlap of the data for all dilute viscoelastic solutions showing an enhancement in convective heat transfer with increasing *Wi*. However, the normalised values of $\overline{Nu}$ for the semi-dilute viscoelastic solution (500-W/SUC) increase more sharply against *Wi* than the dilute solutions. Shear-thinning influences may be significant because of the large shear rates encountered in this

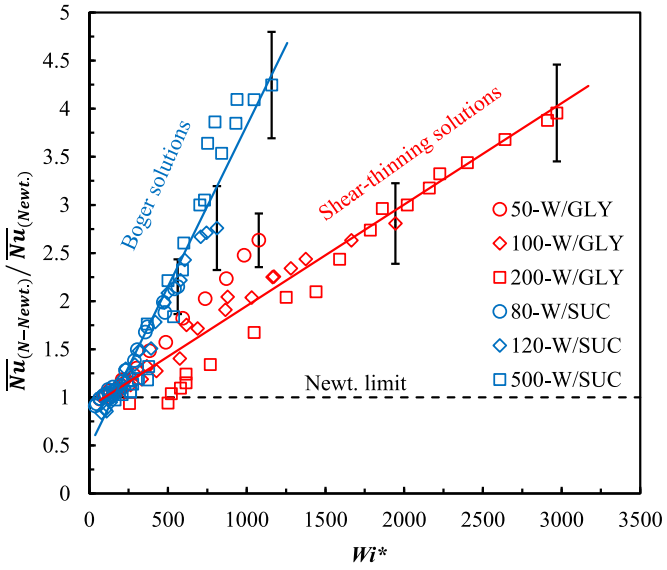

Fig. 14. Normalised Mean Nusselt number, $\overline{Nu}$, versus modified Weissenberg number, Wi^*, for PAA-W/GLY and PAA-W/SUC solutions.

micro-scale flow as might thermal development effects. Therefore, Fig. 14 illustrates the relation between the normalised $\overline{Nu}$ and modified Weissenberg number, Wi^*, which we define as:

$$Wi^* = \left(\frac{W}{L}\right) \mathrm{Pr}\, Wi. \tag{7}$$

The modified Weissenberg number, which represents the ratio of elastic stress to thermal diffusion stress, combines geometric dimensions (depth, W, and path-length, L, of the square serpentine channel), Prandtl number (Pr) and Weissenberg number (Wi) to describe the convective heat transfer under thermally-developing conditions. It is worthwhile to note that the momentum diffusivity for all viscoelastic solutions is much greater than the thermal diffusivity, such that $Pr >> 1$. The experimental results in Fig. 14 show that Boger solutions can enhance convective heat transfer over a Wi^* range of approximately between 250 and 750. While, the shear-thinning solutions need a wide range of Wi^* to enhance convective heat transfer from around 500 to 3250. Essentially, the results are indicating that the mean Nusselt number is a function of both Wi^* and the degree of shear-thinning of the fluids. Generally, the findings in Fig. 14 are consistent for each viscoelastic solution group depending on the rheological characteristics and thermal properties. Overall the collapse against the classical Wi (Fig. 13) is better, especially for dilute solutions.

Differences between the constant viscosity and shear-thinning solutions both in the pressure-drop data (Fig. 10) and in the heat transfer data (Figs. 13 and 14) may be due to a number of different reasons. Firstly we have used the longest relaxation time, determined from small amplitude oscillatory shear data in the limit of low frequency, at the mean film temperature to determine the Weissenberg number. As the data in Fig. 5 shows, however, the relaxation time exhibits frequency/rate dependence and a *characteristic* relaxation time – determined at the mean wall shear rate for example – might offer better collapse of the data. One method to determine such a rate-dependent relaxation time in the non-linear regime is to use first normal-stress difference data as shown in Fig. 6. Unfortunately our attempts to replot the data using this data did not prove successful, most probably as a consequence of the large uncertainty associated with measurements of N_1 for such low concentration fluids. A secondary reason for the differences may be due to the estimate of the viscous stress within the flow which we estimated as a characteristic shear rate (U/W) multiplied by a characteristic viscosity determined at the same shear rate (at the mean film temperature). The use of a simple characteristic shear rate is clearly a simplification as the shear-thinning fluids will have flatter velocity profiles in the laminar regime – and hence higher wall shear rates – and the mean film temperature is only a first order correction. We note also that the relaxation time exhibited different temperature and shear-rate dependence for each of the two fluid types (e.g. constant-viscosity or shear thinning). The activation energy estimates for the two solvents also suggest that the glycerine-based (shear-thinning) solutions are likely to exhibit greater temperature dependence adding further complication to any attempt to collapse the data onto a single curve. Additionally, a conventional "dimensional analysis" approach to the problem would suggest extra dependency with an additional dimensionless group for the shear-thinning fluids (e.g. the n parameter of the Carreau–Yasuda model provided in Table 5). Even the onset of the first purely-elastic instability has recently been shown to be affected by shear-thinning, such that data collapse cannot solely be achieved based on a Weissenberg number alone once shear-thinning becomes significant [47]. Given all of the above issues, the reasonable collapse found against one single dimensionless group, either Wi or Wi^*, for the six different fluids is perhaps not unreasonable.

5. Conclusion

Convective heat transfer and pressure-drop measurements were quantitatively measured using two groups of viscoelastic fluids, namely shear-thinning solutions and approximately constant-viscosity Boger solutions. The thermal boundary conditions were such that the upper wall of the serpentine channel was insulated (adiabatic) and the side walls were maintained at constant temperature. The normalised values of non-dimensional pressure drop in terms of fRe – essentially the pressure-drop normalised by a viscous stress – for the highly-elastic viscoelastic solutions (both shear-thinning and Boger solutions) increase monotonically with increasing Wi and were significantly higher than the Newtonian limit which we attribute to the appearance of so-called "*elastic turbulence*" at high Wi. The elastic turbulence is generated by the non-linear interaction between elastic normal stresses created within the flowing high-molecular-weight polymer solutions and the streamline curvature of the serpentine channel. The elastic turbulence created in the flow of these viscoelastic solutions is able to boost the heat transfer by approximately 200% for low polymer concentrations (50-W/GLY and 80-W/SUC) and reaches up to an increase of 380% for high polymer concentrations (200-W/GLY and 500-W/SUC) whilst keeping the Graetz number sufficiently low such that inertia is essentially negligible. A modified Weissenberg number, defined as the ratio of elastic stress to thermal diffusion stress, is able to approximately collapse the normalised data of mean Nusselt number for each viscoelastic solution group. We suggest that elastic turbulence is therefore a method which can be employed to enhance convective heat transfer and to boost micro-mixing technologies in practical micro-scale applications.

Acknowledgements

Waleed M. Abed gratefully acknowledges the financial support from the higher committee for education development in Iraq (HCED) the Iraqi ministry of higher education and scientific research (under Grant number (D-10-2463) for his Ph.D. study. The authors would like to express appreciation to Dr. Lin Chen (Centre for Materials Discovery, University of Liverpool) for her assistance in measuring specific heat capacity. The authors would like to

thank John Gearing (MD Gearing Scientific Ltd) for his assistance in measuring thermal conductivity. RJP acknowledges funding for a "Fellowship in Complex Fluids and Rheology" from the Engineering and Physical Sciences Research Council (EPSRC, UK) under Grant number (EP/M025187/1).

References

[1] D.D. Carlo, Inertial microfluidics", Lab Chip 9 (2009) 3038–3046, doi:10.1039/b912547g.
[2] A. Groisman, V. Steinberg, Elastic turbulence in a polymer solution flow, Nature 405 (2000) 53–55, doi:10.1038/35011019.
[3] A. Groisman, V. Steinberg, Elastic turbulence in curvilinear flows of polymer solutions, New J. Phys. 6 (2004) 1–48, doi:10.1088/1367-2630/6/1/029.
[4] B.A. Schiamberg, L.T. Shereda, H. Hu, R.G. Larson, Transitional pathway to elastic turbulence in torsional, parallel-plate flow of a polymer solution, J. Fluid Mech. 554 (2006) 191–216, doi:10.1017/S0022112006009426.
[5] A. Groisman, V. Steinberg, Efficient mixing at low Reynolds number using polymer additives, Nature 410 (2001) 905–908, doi:10.1038/35073524.
[6] T. Burghelea, E. Segre, I. Bar-Yosef, A. Groisman, V. Steinberg, Chaotic flow and efficient mixing in a microchannel with a polymer solution, Phys. Rev. E 69 (2004) 066305, doi:10.1103/PhysRevE.69.066305.
[7] F.C. Li, H. Kinoshita, X.B. Li, M. Oishi, T. Fujii, M. Oshima, Creation of very-low-Reynolds-number chaotic fluid motions in microchannels using viscoelastic surfactant solution, Exp. Thermal Fluid Sci. 34 (2010) 20–27, doi:10.1016/j.expthermflusci.2009.08.007.
[8] K. Tatsumi, Y. Takeda, K. Suga, K. Nakabe, Turbulence characteristics and mixing performances of viscoelastic fluid flow in a serpentine microchannel, J. Phys.: Conf. Ser. 318 (2011) 092020, doi:10.1088/1742-6596/318/9/092020.
[9] J. Beaumont, N. Louvet, T. Divoux, M.A. Fardin, H. Bodiguel, S. Lerouge, S. Manneville, A. Colin, Turbulent flows in highly elastic wormlike micelles, Soft Matter 3 (2013) 735–749, doi:10.1039/c2sm26760h.
[10] A.N. Morozov, W. van Saarloos, An introductory essay on subcritical instabilities and the transition to turbulence in visco-elastic parallel shear flows, Phys. Rep. 447 (2007) 112–143, doi:10.1016/j.physrep.2007.03.004.
[11] R.G. Larson, E.S.G. Shaqfeh, S.J. Muller, A purely elastic instability in Taylor–Couette flow, J. Fluid Mech. 218 (1990) 573–600, doi:10.1017/S0022112090001124.
[12] R.J. Poole, B. Budhiraja, A.R. Cain, P.A. Scott, Emulsification using elastic turbulence, J. Non-Newton. Fluid Mech. 177-178 (2012) 15–18, doi:10.1016/j.jnnfm.2012.03.012.
[13] J.P. Hartnett, M. Kostic, Heat transfer to a viscoelastic fluid in laminar flow through a rectangular channel, Int. J. Heat Mass Transf. 28 (6) (1985) 1147–1155, doi:10.1016/0017-9310(85)90122-X.
[14] J.P. Hartnett, Viscoelastic fluids: a new challenge in heat transfer, J. Heat Transf. 114 (1992) 296–303, doi:10.1115/1.2911275.
[15] C. Xie, J.P. Hartnett, Influence of rheology on laminar heat transfer to viscoelastic fluids in a rectangular channel, Ind. Eng. Chem. Res. 31 (3) (1992) 727–732, doi:10.1021/ie00003a012.
[16] S.X. Gao, J.P. Hartnett, Heat transfer behavior of Reiner-Rivlin fluids in rectangular ducts, Int. J. Heat Mass Transf. 39 (6) (1996) 1317–1324, doi:10.1016/0017-9310(95)00041-0.
[17] M.F. Naccache, P.R.S. Mendes, Heat transfer to non-Newtonian fluids in laminar flow through rectangular ducts, Int. J. Heat Fluid Flow 17 (6) (1996) 613–620, doi:10.1016/S0142-727X(96)00062-8.
[18] P. Payvar, Heat transfer enhancement in laminar flow of viscoelastic fluids through rectangular ducts, Int. J. Heat Mass Transf. 40 (3) (1997) 745–756, doi:10.1016/0017-9310(96)00091-9.
[19] S. Syrjälä, Laminar flow of viscoelastic fluids in rectangular ducts with heat transfer: a finite element analysis, Int. Comm. Heat Mass Transf. 25 (2) (1998) 191–204, doi:10.1016/S0735-1933(98)00006-2.
[20] N. Peres, A.M. Afonso, M.A. Alves, F.T. Pinho, Heat Transfer Enhancement in Laminar Flow of Viscoelastic Fluids Through a Rectangular Duct, Congreso de Métodos Numéricos en Ingeniería, Barcelona, Spain, 2009.
[21] R.D. Whalley, W.M. Abed, D.J.C. Dennis, R.J. Poole, Enhancing heat transfer at the micro-scale using elastic turbulence, Theor. Appl. Mech. Lett. 5 (2015) 103–106, doi:10.1016/j.taml.2015.03.006.
[22] B. Traore, C. Castelain,T. Burghelea, Efficient heat transfer in a regime of elastic turbulence, J. Non-Newton. Fluid Mech. 223 (2015) 62–76, doi:10.1016/j.jnnfm.2015.05.005.
[23] W.M. Abed, R.D. Whalley, D.J.C. Dennis, R.J. Poole, Numerical and experimental investigation of heat transfer and fluid flow characteristics in a micro-scale serpentine channel, Int. J. Heat Mass Transf. 88 (2015) 790–802, doi:10.1016/j.ijheatmasstransfer.2015.04.062.
[24] A.R. Chandrupatla, V.M. Sastri, Laminar forced convection heat transfer of a non-Newtonian fluid in a square duct, J. Heat Mass Transf. 20 (1977) 1315–1324, doi:10.1016/0017-9310(77)90027-8.
[25] R.B. Bird, R.C. Armstrong, O. Hassager, Dynamics of Polymeric Liquids, second ed., John Wiley and Sons Inc., New York, 1987.
[26] D.V. Boger, A highly elastic constant-viscosity fluid, J. Non-Newton. Fluid Mech. 3 (1977/1978) 87–91, doi:10.1016/0377-0257(77)80014-1.
[27] M.P. Escudier, I.W. Gouldson, A.S. Pereira, F.T. Pinho, R.J. Poole, On the reproducibility of the rheology of shear thinning liquids, J. Non-Newton. Fluid Mech. 97 (2001) 99–124, doi:10.1016/S0377-0257(00)00178-6.
[28] K. Yasuda, R.C. Armstrong, R.E. Cohen, Shear flow properties of concentrated solutions of linear and star branched polystyrenes, Rheol. Acta 20 (1981) 163–178, doi:10.1007/BF01513059.
[29] R. Lapasin, S. Pricl, Rheology of Industrial Polysaccharides: Theory and Applications, Blackie Academic & Professional, London, 1995.
[30] A.B. Rodd, D.E. Dunstan, D.V. Boger, Characterisation of xanthan gum solutions using dynamic light scattering and rheology, Carbohydr. Polym. 42 (2) (2000) 159–174.
[31] H.A. Barnes, J.F. Hutton, K. Walters, An Introduction to Rheology, Elsevier Science Limited, 1989.
[32] R.G. Larson, The Structure and Rheology of Complex Fluids, Oxford, New York NY, 1999.
[33] V. Tirtaatmadja, G.H. McKinley, J.J. Cooper-White, Drop formation and breakup of low viscosity elastic fluids: effects of molecular weight and concentration, Phys. Fluids 18 (2006) 043101.
[34] L.E. Rodd, J.J. Cooper-White, D.V. Boger, G.H. McKinley, Role of the elasticity number in the entry flow of dilute polymer solutions in micro-fabricated contraction geometries, J. Non-Newton. Fluid Mech. 143 (2007) 170–191, doi:10.1016/j.jnnfm.2007.02.006.
[35] J.E. Mark, Polymer Data Handbook, second ed., Oxford University Press, Inc., 2009.
[36] K. Walters, Rheometry, Chapman and Hall, 1975.
[37] D.A. Ditmars, S. Ishihara, S.S. Chang, G. Bernstein, E.D. West, Enthalpy and heat-capacity standard reference material - synthetic sapphire (ALPHA-AL2O3) from 10 to 2250 K, J. Res. Natl. Bur. Stand. 87 (2) (1982) 159–163, doi:10.6028/jres.087.012.
[38] R.P. Chhabra, J.F. Richardson, Non-Newtonian Flow and Applied Rheology: Engineering Applications, second ed., Butterworth-Heinemann, Elsevier Science Limited, 2008 ISBN: 978-0-7506-8532-0.
[39] W.Y. Lee, Y.I. Cho, J.P. Hartnett, Thermal conductivity measurements of non-Newtonian fluids, Lett. Heat Mass Transf. 8 (1981) 255–259, doi:10.1016/0094-4548(81)90039-4.
[40] Glycerine Producers' Association, Physical Properties of Glycerine and its Solution, Glycerine Producers' Association, 1963.
[41] M. Werner, A. Baars, F. Werner, C. Eder, A. Delgado, Thermal conductivity of aqueous sugar solutions under high pressure, Int. J. Thermophys. 28 (2007) 1161–1180, doi:10.1007/s10765-007-0221-z.
[42] M. Asadi, Beet-Sugar Handbook, John Wiley & Sons, Inc., 2011 ISBN: 978-0-471-76347-5.
[43] F.P. Incropera, D.P. DeWitt, T.L. Bergman, A.S. Lavine, Introduction to Heat Transfer, fifth ed., John Wiley and Sons, New York, 2005.
[44] W.R. Dean, Fluid motion in a curved channel, Proc. R. Soc. Lond. 121 (787) (1928) 402–420, doi:10.1098/rspa.1928.0205.
[45] R.J. Poole, M.A. Alves, A. Lindner, Viscoelastic secondary flows in serpentine channels, J. Non-Newton. Fluid Mech. 201 (2013) 10–16, doi:10.1016/j.jnnfm.2013.07.001.
[46] J. Zilz, R.J. Poole, M.A. Alves, D. Bartolo, B. Levache, A. Lindner, Geometric scaling of a purely elastic flow instability in serpentine channels, J. Fluid Mech. 712 (2012) 203–218, doi:10.1017/jfm.2012.411.
[47] L. Casanellas, M.A. Alves, R.J. Poole, S. Lerouge, A. Lindner, "Stabilizing effect of shear thinning on the onset of purely-elastic instabilities in serpentine microflows". Soft Matter. To appear.